Southern California Permanent GPS Geodetic Array: Spatial filtering of daily positions for estimating coseismic and postseismic displacements induced by the 1992 Landers earthquake

Shimon Wdowinski,[1] Yehuda Bock, Jie Zhang, Peng Fang, and Joachim Genrich

Cecil H. and Ida M. Green Institute of Geophysics and Planetary Physics, Scripps Institution of Oceanography
La Jolla, California

Abstract. The June 28, 1992 (M_W=7.3) Landers, California, earthquake was the first earthquake to be surveyed by a continuously operating Global Positioning System (GPS) array. The coordinate time series of seven sites are evaluated for station displacements during an interval of 100 days centered on the day of the earthquake. We employ a new spatial filtering technique that removes common-mode errors from the coordinate time series. This approach provides precise estimates of site-specific displacements compared to the cumbersome method of analyzing baselines between pairs of stations. All sites indicate significant coseismic horizontal displacements of 5–65 mm with uncertainties of 1–2 mm. Horizontal displacements are in general agreement with elastic dislocation models, in particular for sites closer to the epicenter. Vertical displacements range from -13 to +7 mm with uncertainties of 2–4 mm. The observed vertical displacements in all cases show 5–10 mm more subsidence than expected from geodetic and seismic/geologic models. Significant postseismic horizontal displacements totaling 6±2 mm (10–20% of the coseismic displacement) are detected at the three sites closest to the epicenter. These displacements are modeled as a short-term exponential relaxation with a decay time of 22±10 days superimposed on a longer-term linear interseismic trend. Scaling the observed coseismic and postseismic displacements at one of the sites with the distance to the epicenter provides a measure of site strain, which agrees well with the direction and magnitude determined from more precise laser strain meter data. The time series do not show any detectable preseismic displacements.

Introduction

The June 28, 1992, Landers earthquake was the strongest earthquake (M_W=7.3) to strike southern California in the past 40 years. It ruptured the crust along 85 km and displaced it by up to 7 m in less than 24 s [*Kanamori et al.*, 1992]. The earthquake ruptured the surface along 70 km and displaced it by up to 6.5 m in a predominantly dextral motion [*Landers Earthquake Response Team*, 1993]. The mainshock was followed by more than 15,000 aftershocks, which were concentrated along the ruptured fault (Figure 1). The largest aftershock, the Big Bear earthquake (M_S=6.5), occurred 3 hours after the Landers mainshock on a separate fault nearly orthogonal to the main ruptured faults. It ruptured the crust along 20 km and caused an average of 0.5 m of sinistral motion [*Hauksson et al.*, 1992] but did not rupture the surface. The Landers event measurably displaced the crust in southern California within an epicentral radius of about 300 km.

The large surface displacements induced by the Landers earthquake were observed by several complementary geodetic techniques. A continuously monitoring Global Positioning System (GPS) geodetic network, the southern California Permanent GPS Geodetic Array (PGGA) [*Bock*, 1991], provided for the first time, spatial, and temporal details of crustal movements before, during, and after a major earthquake [*Blewitt et al.*, 1993; *Bock et al.*, 1993]. Reoccupation of geodetic benchmarks by GPS and electronic distance measurements (EDM) provided accurate measurements of near-field coseismic displacements [*Hudnut et al.*, 1994; *Freymueller et al.*, 1994]. Additional GPS surveys of local sites 2–6 months later provided a description of near-field postseismic deformation [*Shen et al.*, 1992, 1994]. Strain meters and tiltmeters recorded the short-term strain accumulation before and after the Landers earthquake and detected both coseismic and postseismic deformation [*Johnston et al.*, 1994; *Wyatt et al.*, 1994]. A broad-scale map view of the Landers coseismic and postseismic displacement field was obtained by interferometric synthetic aperture radar (INSAR) with unprecedented spatial resolution [*Massonnet et al.*, 1993, 1994; *Zebker et al.*, 1994].

Bock et al. [1993] analyzed continuous GPS data collected before and after the Landers earthquake and detected significant far-field surface displacements at five PGGA sites. In this study we reanalyze the data of these five sites, including two sites not analyzed previously, to reevaluate the far-field displacements. The GPS data are reprocessed with an improved mathematical model, more precise satellite orbit estimation,

---

[1]Now at Department of Geophysics and Planetary Sciences, Tel Aviv University, Ramat Aviv, Israel.
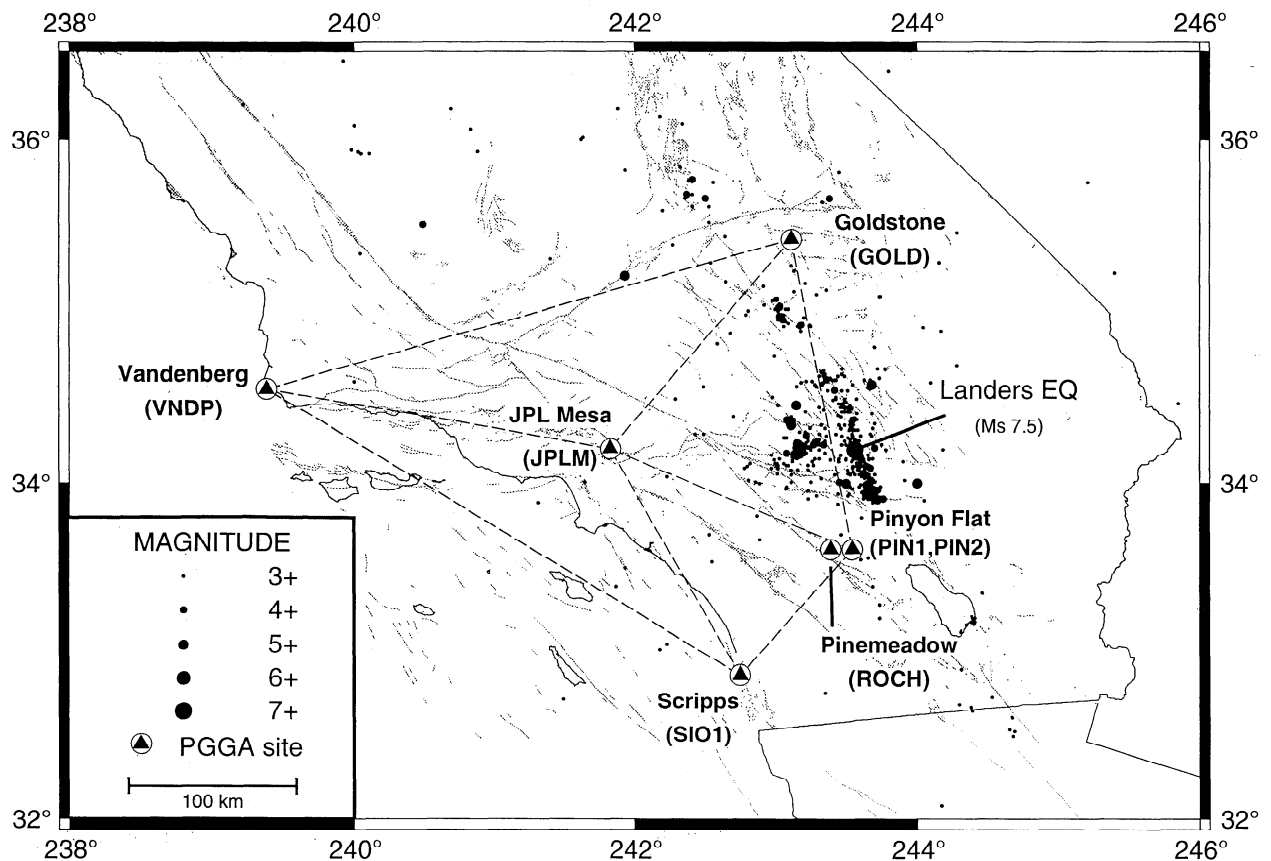
Figure 1. Map of southern California showing seismicity during 1992–1993, the location of the Landers earthquake epicenter, and the Permanent GPS Geodetic Array (PGGA) sites. Dashed lines present the 1992 geometry of the PGGA.

integer-cycle phase ambiguity resolution, and an updated terrestrial reference frame. In a postprocessing step, we apply a new spatial filtering technique that increases significantly the signal-to-noise ratio of estimated site positions. This additional step enables us to resolve total surface displacement into its coseismic and postseismic components site-by-site, rather than by cumbersome analysis of relative displacements between pairs of sites.

The coseismic and short-term postseismic displacements of the PGGA sites induced by the Landers earthquake are the focus of this study. Interseismic displacements are described in detail by *Bock et al.* [this issue] and *Zhang et al.* [this issue].

Observations

This study makes use of continuous GPS measurements from seven sites that were active during 100 days centered on the Landers earthquake. Two sites are located 50 m apart at the Piñon Flat Observatory (Figure 1). One site (SIO1) was taken off line permanently only 2 weeks before the Landers earthquake and replaced without interruption by a nearby site (SIO2) using the same equipment. The relative baseline vector between these two sites was determined with mm precision by simultaneous GPS measurements with identically configured GPS systems [*Bock et al.*, this issue]; thus we were able to merge the two disjoint time series into one which we refer to throughout this paper as "SIO1." Five of the sites (GOLD, JPLM, PIN1, SIO1, and VNDP) were equipped with Rogue SNR-8 precise P-code receivers and Dorne-Margolin antenna elements with choke rings. Two of the sites (PIN2 and ROCH)

were equipped with Trimble 4000 SST receivers with codeless L2-carrier tracking and Trimble 4000 SST L1/L2 geodetic antennas [*Happer et al.*, 1991]. Most sites have highly stable geodetic monuments especially designed for the PGGA [*Wyatt et al.*, 1989; *Bock et al.*, this issue], except for JPLM where the monument is located over an existing mobile very long baseline interferometry (VLBI) mark and for the NASA Deep Space Network site at Goldstone (GOLD) located on a 25 m steel tower.

Once a day, 24 hours of observed GPS dual-frequency phase and pseudorange data are automatically collected from each PGGA site. The data are analyzed with the GAMIT [*King and Bock*, 1995] and GLOBK [*Herring*, 1995] software packages providing three-dimensional site positions in the International Terrestrial Reference Frame 1993 (ITRF93) [*Boucher et al.*, 1994]. Details of PGGA operations and analysis procedures are discussed by *Bock et al.* [this issue]. The Landers main event occurred on day 180 (June 28, 1992) at 1158 UTC, the Big Bear earthquake followed at 1507 UTC. Therefore, the data from this day were analyzed in two separate GAMIT solutions of 24 hours each. The first segment consisted of the global data collected over 24 hours, and all PGGA data collected before 1158 (nearly 12 hours of data), and the second segment consisted of the same global data but only the PGGA data collected after 1507 UTC (nearly 9 hours of data). The data between the two earthquakes were not included in the analysis.

The "raw" time series of three-dimensional site positions are shown in Figure 2. The day of the earthquakes, is denoted by a vertical dotted line. The error bars are computed from the

Raw station positions (mm)
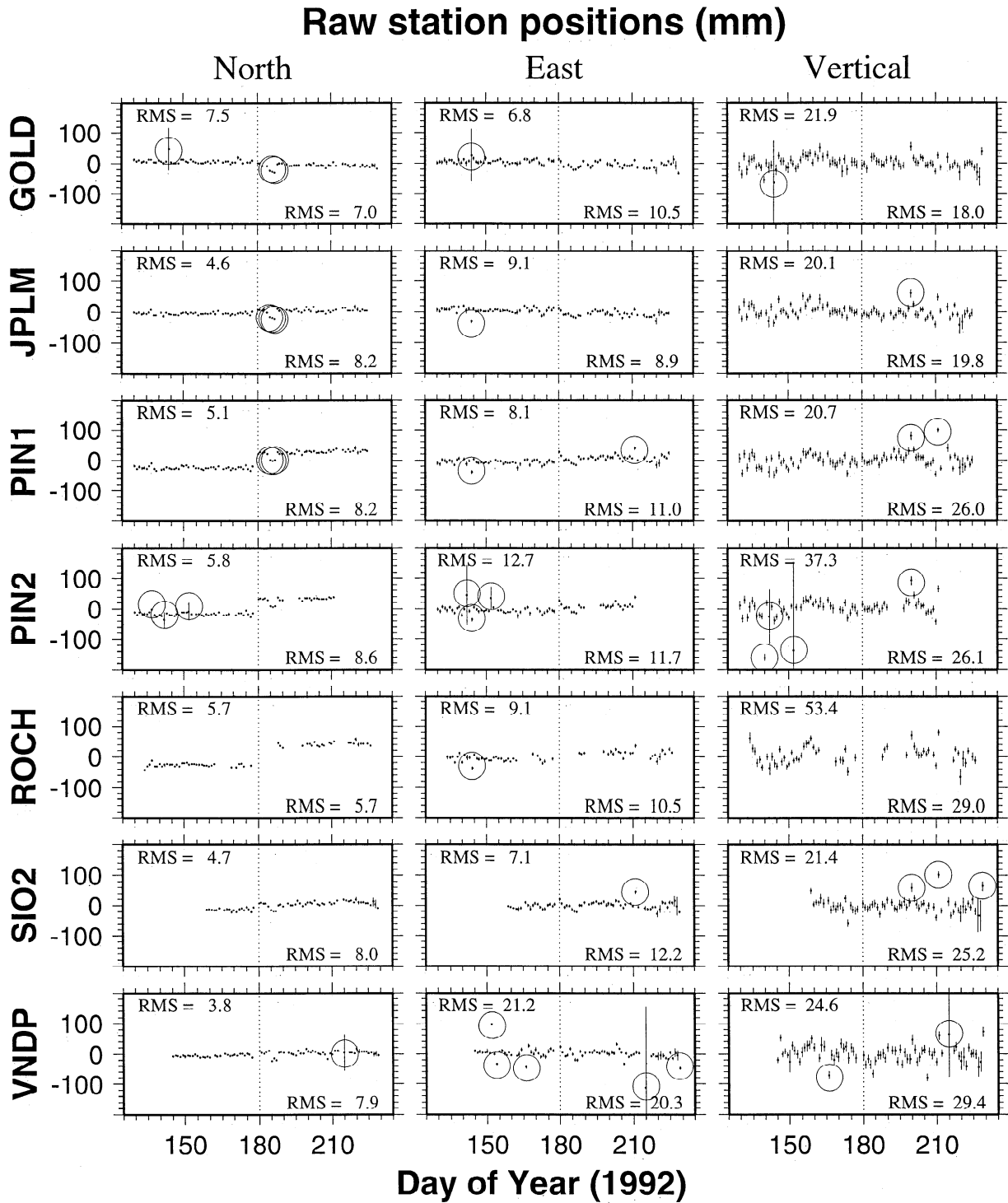
Figure 2. Raw 100-day time series of daily three-dimensional positions of PGGA sites with respect to the ITRF93. The vertical dotted line indicates the day of the Landers earthquake (day 180). Root-mean-square (RMS) values are computed for the detrended series before and after this day. Error bars indicate formal (1σ) standard errors from the GAMIT/GLOBK analysis. Outliers are indicated by circles. Note that three points in the north component a few days after the earthquake day are marked as outliers at three of six sites, and exhibit like behavior at the sixth site (PIN2) (these points are missing from the seventh site, ROCH). The three points are retained in the stacking procedure.

GLOBK smoothing filter described by *Bock et al.* [this issue], by scaling the 1-σ daily component uncertainties by the overall chi-square per degree of freedom. Analysis of a longer span of PGGA data by *Zhang et al.* [this issue] indicates colored noise with fractal white noise characteristics implying that the error bars should be multiplied by about a factor of 2–3.

Improved Time Series

It is important to identify and remove features in the time series that are clearly not due to the earthquake deformation cycle. As a first step, we eliminate data outliers from all three components (see Figure 2). We define as outliers points (1) with error bars larger than 3 times the root-mean-square (RMS) scatter in any of the components or (2) that deviate from the mean of the series by more than 3 times the RMS scatter. Outliers of the first kind are due to an incomplete observation span (significantly less than 24 hours) at a particular site. Outliers of the second kind detected in the horizontal components are thought to be due to erroneous or incomplete choices of integer-cycle phase ambiguities (at the GAMIT analysis stage), since they appear primarily in the more sensitive east component. Those in the vertical component are thought to be due to orbital and reference frame errors since they are common to all sites. These operations are performed independently on the data segments before and after the earthquake, and in an iterative manner until all outliers are eliminated. Although the procedure detected three outliers in the north component in three out of the seven sites (Figure 2, days 184–186), we do not eliminate them from the time series because they show a systematic pattern that can be treated by spatial filtering described below. The time series, cleaned of outliers (except for three data points in the north component just after the earthquake), are shown in Figure 3a at an enhanced scale.

The "cleaned" time series are characterized by (1) discontinuous position changes at day 180, the day of the earthquakes, (2) a long-term continuous change in position before and after day 180, and (3) short-term position changes, which reflect the daily repeatability of the GPS observations. Tectonic signals are considered to be either abrupt changes in position (coseismic displacements) or longer-term continuous changes (e.g., interseismic, preseismic, and postseismic displacements). Therefore the day-to-day position changes can be considered as a daily noise superimposed on the longer-term tectonic signals. In order to characterize this noise level, we detrend the series of the horizontal components according to the long-term displacement rates (Figure 3a, solid lines) determined from the longer PGGA time series by *Zhang et al.* [this issue], for the 19 month time series between the Landers and the January 19, 1994 Northridge earthquakes. The intercepts of the long-term trends (solid lines in Figure 3a) are determined by weighted least squares fitting of the data on each side of day 180 to a straight line with fixed long-term-determined slope for horizontal components and zero slope for vertical components. We use the long-term displacement rate, because a least-square fitting of the 50-day-long time series, before and after the earthquake, is too sensitive to the daily noise, and may vary by as much as 10 mm/yr from the long-term rate. The vertical station velocities are assumed to be zero because of the large scatter in the vertical daily positions.

The detrended time series are characterized by RMS scatter of 4–8 mm in the north, 8–12 mm in the east, and 15–30 mm in the vertical component (Figure 3a). This scatter represents daily repeatability for the 50-day time series and is larger than the error bars resulting from the GLOBK analysis. It is also larger than the day-to-day scatter of the relative position (baseline vector) between any two sites (Figure 4), indicating the presence of a common-mode positioning error that is eliminated by differencing the positions of the two stations. This signature is apparent at all sites when the various components are aligned (or "stacked"), particularly in the east and vertical components (Figure 3a). We assume that this signature (COMM in Figure 3a) is a common bias for all sites and is most likely nontectonic because of its large regional extent. Therefore it is justified to eliminate this bias from the data series which we do in the following 3-step procedure.

Detrending. By simplified linear regression, determine the component intercept that best fits the data given the postearthquake site velocities calculated from the longer time series analyzed by *Zhang et al.* [this issue] (solid lines in Figure 3a). For each day d and site s calculate the residual, i.e., the difference in position between the observed and predicted values,

$$\varepsilon_s(d) = O^s(d) - C^s(d) \tag{1}$$

Stacking. Calculate the common-mode bias on a day-by-day basis by averaging the values from all S sites

$$\bar{\varepsilon}(d) = \frac{\sum_{s=1}^{S} \varepsilon_s(d)}{S} \tag{2}$$

If $S=1$, the data point from the one site is deleted from the corresponding time series. The determination of the common mode should improve with the number of sites. However, Figure 3a shows that for each component the common-mode bias, which was obtained by stacking two to seven sites, shows an almost uniform scatter, indicating a minor influence on the number of sites used by the algorithm.

Filtering. For each site, subtract the common-mode error from the observed position $O_s(d)$ to obtain the filtered position $\hat{O}_s(d)$

$$\hat{O}_s(d) = O_s(d) - \bar{\varepsilon}(d) \tag{3}$$

In case of an abrupt change (step function) in the time series, e.g., coseismic displacement, the algorithm is applied separately to the time series segments before and after the day of the change. Apparent postseismic displacement requires special consideration. Sites that are suspected of experiencing postseismic displacement (PIN1, PIN2, ROCH) do not participate in the stacking for the period affected. However, we subtract from those sites the common-mode bias calculated from the remainder of the sites that are thought not to have experienced postseismic deformation.

The "filtered" time series, which are shown in Figure 3b, exhibit significantly reduced RMS scatter compared to the cleaned time series. The RMS scatter ranges from 2–4 mm in the north component, 3–7 mm in the east component, and 5–23 mm in the vertical component. Thus the filtered time series for each site will generally have lower scatter than individual baseline (relative position) series, assuming that the common signal dominates the errors at each site. Baseline components are unchanged because the filtering algorithm removes the same value from all sites.

Every PGGA site experienced significant coseismic displacement induced by the Landers earthquake, while only three sites experienced postseismic displacement. Our

Cleaned station positions (mm)
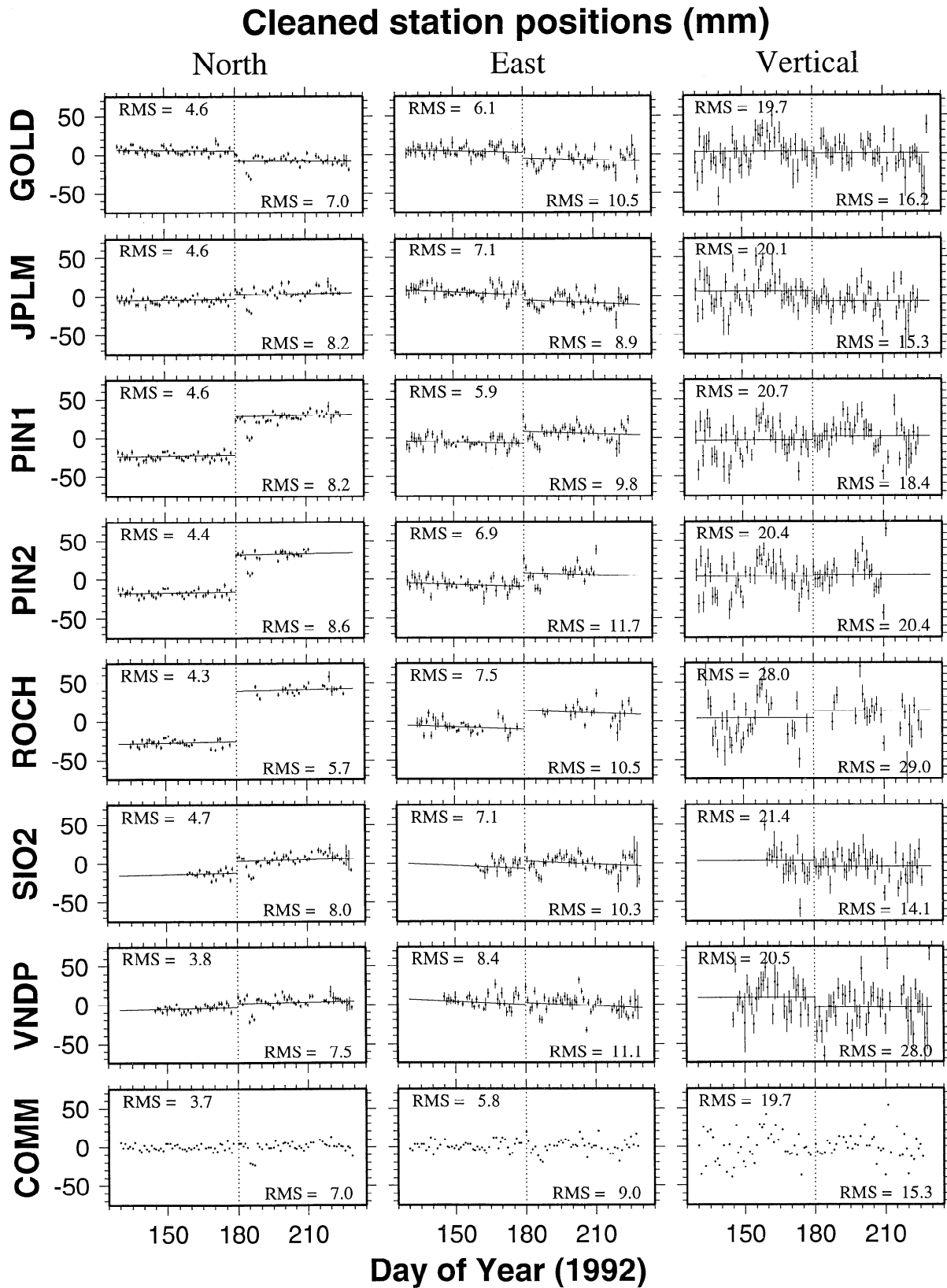
Figure 3a. Cleaned (data outliers removed except for three data points in the north component just after the earthquake) 100-day time series of daily three-dimensional positions of the PGGA sites with respect to the ITRF93 and their common- mode ("COMM") signal. Note the vertical scale difference in all components compared to Figure 2. The vertical dotted line indicates the day of the Landers earthquake (day 180). The solid lines represent the long-term interseismic displacement rates that best fit the data (see text). Root-mean-square (RMS) values are computed for the detrended cleaned series before and after this day. The error bars are computed from the GLOBK smoothing filter, by scaling the 1σ daily component uncertainties by the overall chi-square per degree of freedom.

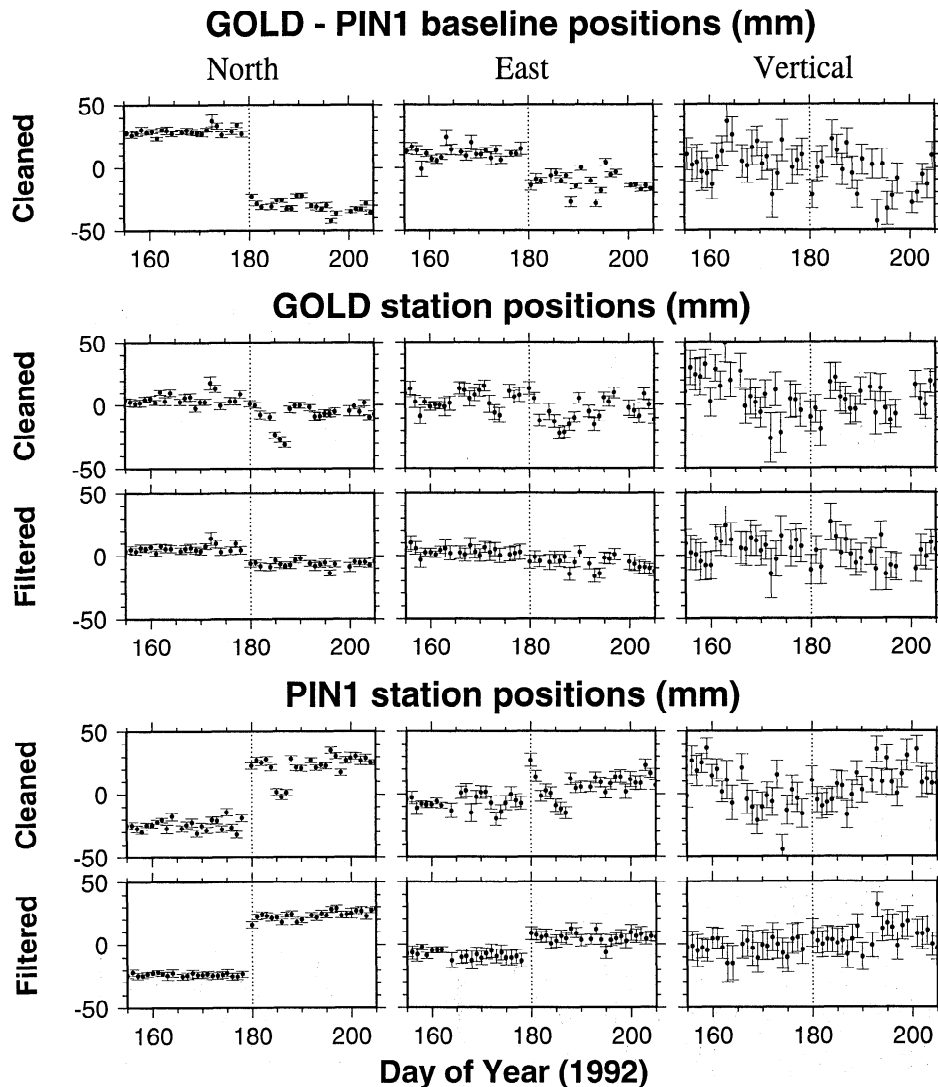# Filtered station positions (mm)
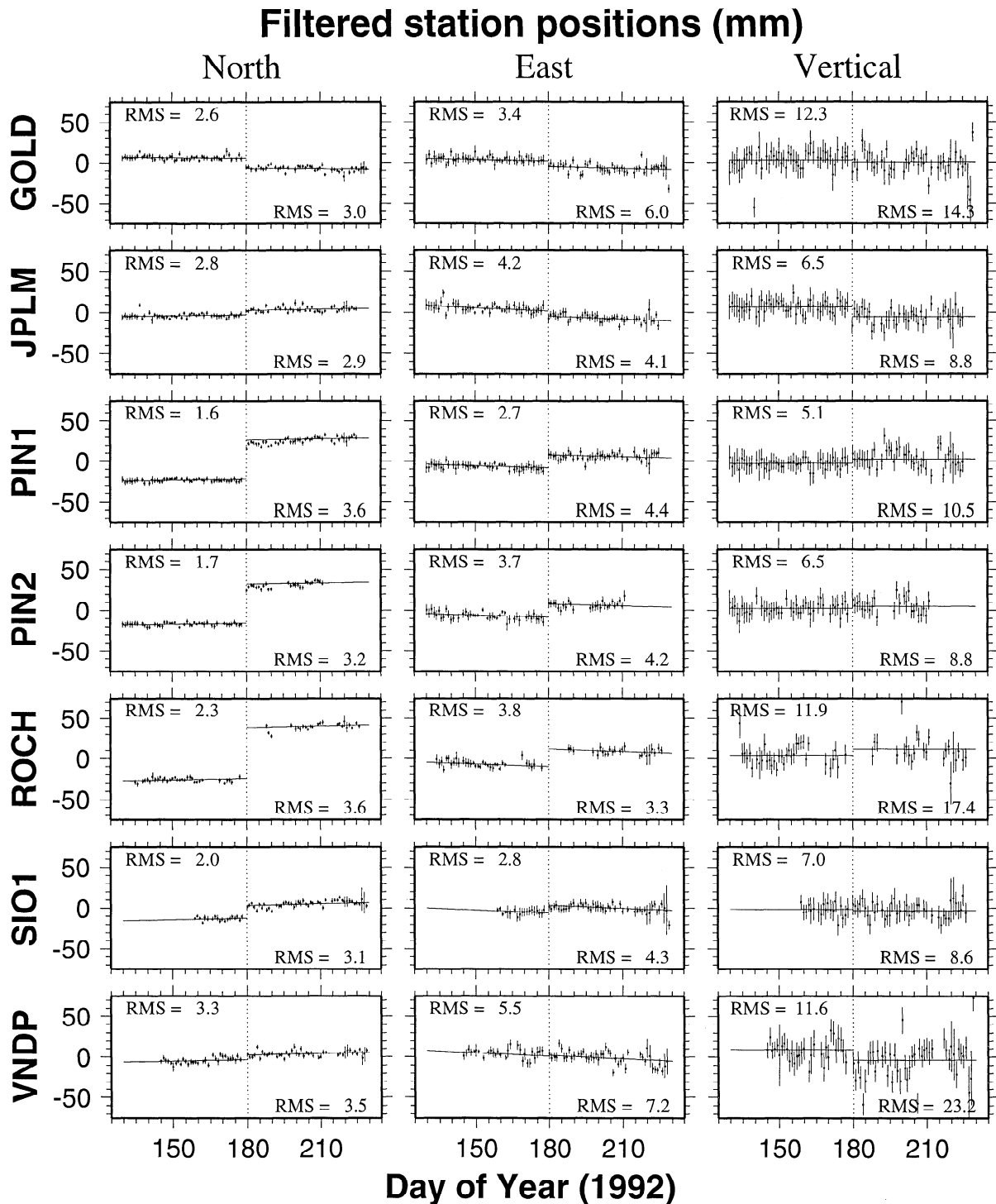
Figure 3b. Spatially filtered 100-day time series of daily three-dimensional positions of PGGA sites offset daily with respect to the ITRF93 by the common-mode bias estimated for a particular day.

stacking algorithm reduces the RMS scatter of the time series and therefore provides much higher resolution for detecting transient signals on a site-by-site basis without having to fix the position of any site in the regional array. The traditional way of analyzing baselines to detect displacement is not convenient for determining the amount of displacement at each individual site. In the next section, we apply our stacking algorithm to the PGGA data and demonstrate the power of this approach.

Seismically Induced Site Displacements

Crustal deformation of tectonically active areas is generally described in terms of a cycle that is composed of the following four stages: interseismic, preseismic, coseismic, and postseismic. The PGGA provides, for the first time, sufficient temporal resolution to examine actual surface deformation for all stages of a major earthquake. The 100-day time series described in this study do not provide sufficient resolution to

GOLD - PIN1 baseline positions (mm)

Figure 4. (top) Time series of the baseline GOLD-PIN1, (middle) cleaned and filtered station positions of GOLD, and (bottom) PIN1. Postseismic displacement was observed in the north component of the baseline during the 10–14 days that followed the earthquake. The cleaned series are characterized by a noise level that does not allow detection of postseismic displacements.

study the interseismic stage but allow a rigorous examination of the deformation before, during, and after the Landers earthquake. Interseismic displacements between the Landers and Northridge earthquakes are investigated and described by *Bock et al.* [this issue] and *Zhang et al.* [this issue] for the longer PGGA time series.

Coseismic Displacements

Analysis of the PGGA time series by *Zhang et al.* [this issue] indicates that uncorrelated GPS measurement error (white noise) is 1–3 mm for a single daily measurement of each horizontal component and 4–10 mm for the vertical component. To determine coseismic deformation, one approach is to average a short segment of daily data points (~30 days) before and after the event and compute the difference as was done by *Blewitt et al.* [1993] and *Bock et al.* [1993]. In this case, one chooses to ignore the insignificant interseismic deformation (and colored noise errors) that have accumulated over this short period. This approach is complicated, however, by any postseismic deformation. In

this case, the coseismic deformation can be computed indirectly by subtracting the postseismic displacement from the total displacement. However, computing the total displacement (the sum of coseismic and postseismic displacement) requires data after the event and detrending of the daily positions before and after the earthquake, after removing the data affected by postseismic deformation. Therefore a more general and rigorous approach to estimating coseismic deformation is to properly detrend the data sets before and after the earthquake, or in other words to compute the interseismic deformation. Here we detrend the time series using the postearthquake displacement rates estimated by *Zhang et al.* [this issue].

The determination of coseismic deformation can be formulated as a linear regression problem. That is, the coseismic deformation is computed by subtracting the abscissa intercepts before and after the earthquake (and ignoring data points affected by postseismic deformation), such that

$$A_{coseismic} = x_0(posteq) - x_0(preeq) \qquad (4)$$

and

$$\sigma^2_{\text{coseismic}} = \sigma^2_{x_0}(\text{preeq}) + \sigma^2_{x_0}(\text{posteq}) \tag{5}$$

Zhang et al. [this issue] (see their appendix A) show that the variance of the coseismic displacement estimate is given approximately by

$$\sigma^2_{\text{coseismic}} \simeq \left(\frac{4a_1^2}{N_1}\right)_{\text{preeq}} + \left(\frac{4a_2^2}{N_2}\right)_{\text{posteq}} \tag{6}$$

where a denotes uncorrelated position error from 24-hours of GPS observations, and N denotes the number of daily measurements. The subscripts 1 and 2 denote preearthquake and postearthquake values, respectively. We have ignored low-frequency colored noise in the time series [*Zhang et al.*, 1997] since its cumulative effect is negligible for the 50 consecutive days before and after the earthquake. This formulation assumes a steady (but not necessarily equal) rate of interseismic deformation before and after the earthquake and that there exists no preseismic deformation. Considering that a = 1–2 mm for horizontal components [*Zhang et al.*, this issue] we require about 3–6 weeks of data before and after an earthquake to estimate coseismic deformation with a precision of about 1 mm, at the 95% confidence level. The vertical component is about a factor of 2–3 times worse.

Horizontal component. We compute the coseismic displacements at each site and for each position component from the 100-day filtered time series using (6). The calculated coseismic displacements are evident in Figure 3b as the offsets between the trended lines before the earthquake and those after the earthquake. The detected horizontal coseismic displacements are summarized in Table 1 and shown in Figure 5a. The only time series that require further analysis are the north components of PIN1, PIN2, and ROCH, whose total seismic displacements point to a significant postseismic component.

Vertical component. Unlike the horizontal time series, the vertical time series are not detrended by the rates computed by *Zhang et al.* [this issue] because the estimated vertical rates lie within their uncertainties. Rather we assume zero vertical velocity before and after the Landers earthquake. According to earthquake dislocation models we expect to see detectable vertical coseismic displacements of magnitudes as large as 15–20 mm at some of the sites (Table 2). However, the vertical coseismic displacements suggest that all sites have been displaced 5–10 mm less than expected from the model displacements [*Bock et al.*, 1993]. Furthermore, the vertical displacement of VNDP (-13.0 ± 6.3 mm), for example, is unrealistically high considering its distance from the epicenter. A visual examination of the vertical time series (Figure 3) indicates that we may have neglected significant higher-frequency temporal correlations which are not apparent in the horizontal series. The short-term temporal correlations are probably due to some complex combination of site-specific unmodeled multipath, atmospheric refraction, antenna phase center, and tidal effects whose error characteristics are beyond the scope of this paper.

To obtain nevertheless a realistic estimate of the vertical coseismic offsets and their uncertainties we resort to robust estimation, as outlined by *Press et al.* [1988]. We assume that the vertical data are equally weighted before and after the earthquake. This condition is reasonable considering that the GPS constellation and the daily position estimation algorithms were uniform throughout this 100-day period. The function to be minimized for the line fitting problem is

$$\sum_{i=1}^{N} \left| y_i - x_0 - rx_i \right| \tag{7}$$

which yields a robust estimate for the line intercept x_0. It is simply the median of the daily positions for fixed r,

$$\hat{x}_0 = \text{median} \{y_i - rx_i\} = \text{median} \{y_i\} \; ; r = 0 \tag{8}$$

Table 1. Comparison of Observed and Model Horizontal Coseismic Displacements

Site Code	Component	Observed Displacements, mm				Model Displacements, mm	
		This Study	Bock et al. [1993]	Blewitt et al. [1993]	Freymueller et al. [1994]	Geodetic	Seismic/Geologic
GOLD	North	-12.9 ± 1.2	-14.6 ± 1.4	-11 ± 1	-12.3 ± 3	-15.8	-17.6
	East	-7.1 ± 1.6	-8.0 ± 2.4	-5 ± 2	5.0 ± 7	-9.5	-8.5
JPLM	North	5.3 ± 1.2	3.4 ± 1.3	7 ± 1	7.3 ± 3	4.9	4.7
	East	-6.1 ± 1.5	-14.7 ± 2.4	-9 ± 2	-4.6 ± 6	-12.8	-13.4
PIN1	North	41.5 ± 2.0	—	—	—	46.6	42.8
	Total[*] North	47.5 ± 1.2	45.6 ± 1.2	46 ± 1	52.0 ± 3	—	—
	East	16.1 ± 1.2	14.0 ± 2.1	19 ± 2	23.1 ± 6.5	17.5	16.2
PIN2	North	40.0 ± 2.0	—	—	—	46.6	42.9
	Total[*] North	46.7 ± 1.3	—	—	—	—	—
	East	16.5 ± 1.7	—	—	—	17.5	16.3
ROCH	North	57.0 ± 2.0	—	—	—	59.1	58.7
	Total[*] North	63.0 ± 1.6	—	—	64.0 ± 4	—	—
	East	21.4 ± 1.7	—	—	26.0 ± 8	20.2	19.2
SIO1	North	15.7 ± 1.3	13.0 ± 1.7	—	19.0 ± 4	14.8	15.1
	East	9.2 ± 1.3	10.1 ± 2.8	—	15.0 ± 8	5.9	6.0
VNDP	North	5.2 ± 1.6	4.5 ± 1.6	—	—	1.0	0.9
	East	1.1 ± 2.3	-4.1 ± 2.5	—	—	-3.0	-3.0

The geodetic model is based on near-field campaign GPS measurements [*Hudnut et al.* 1994]. The seismic/geologic model is based on surface faulting and seismic fault plane solutions [*Bock et al.*, 1993]. Uncertainties are 1σ values.
[*]Total displacements are the sum of coseismic and postseismic displacements.
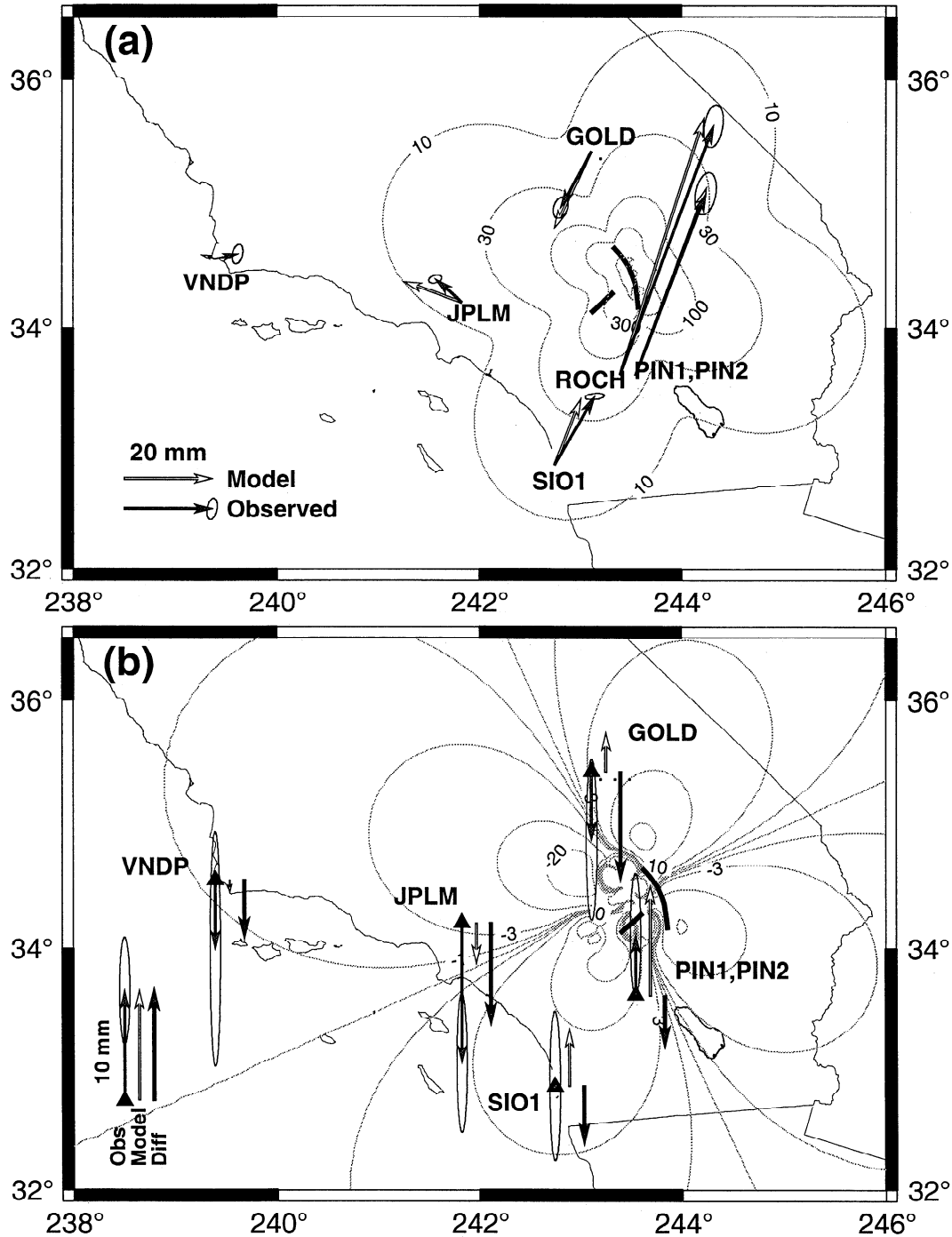
Figure 5. (a) Observed (solid arrows) and modeled (open arrows) horizontal coseismic displacements at the PGGA sites, with 95% confidence ellipses. The contours (in millimeters) show the magnitude of the horizontal displacement field predicted by a dislocation model that assumes seven linear segments describing the rupture geometry of the Landers and Big Bear earthquakes (thick lines). Details of the model are described by *Bock et al.* [1993]. (b) Observed (by robust estimation) and modeled vertical displacements at PGGA sites, including 95% confidence error bars. Differences ("Diff") between observed and model displacements are indicated by thick arrows.

with

$$\hat{\sigma}_{x_0} = \frac{\sum_{i=1}^{N} \left| y_i - \text{median}\{y_i\} \right|}{N-1} \qquad (9)$$

We compute the vertical coseismic offsets by differencing the median of the daily vertical components before and after the earthquake and estimate the uncertainty by substituting (9) for

a in (6). This is only an approximation since (6) was derived assuming only white noise, while neglecting lower-frequency colored noise.

The results of robust estimation of the vertical coseismic displacements are presented in Table 2 and shown in Figure 5b. The scatters in the vertical displacements of PIN1, PIN2, and ROCH are less than the weighted least squares estimator,

Table 2. Comparison of Observed and Model Vertical Coseismic Displacements

| Site Code | Estimator | Observed Displacements (O), mm | | | Model Displacements (M), mm | | O-M, mm |
		This Study	Bock et al. [1993]	Blewitt et al. [1993]	Seismic/ Geologic	Geodetic	This Study - S/G Model
GOLD	least squares	-2.7 ± 4.8	6.0 ± 5.6	-4 ± 5	3.6	3.7	-6.3
	robust	-6.2 ± 3.0	—	—			-9.8
JPLM	least squares	-11.9 ± 2.8	0*	-8 ± 5	-3.7	-4.0	-8.2
	robust	-12.8 ± 2.6	—	—			-9.1
PIN1	least squares	5.0 ± 2.7	9.6 ± 6.4	8 ± 5	10.1	13.3	-5.1
	robust	5.7 ± 1.9	—	—			-4.4
PIN2	least squares	2.9 ± 3.3	—	—	10.1	13.3	-7.2
	robust	5.6 ± 2.3	—	—			-4.5
ROCH	least squares	7.9 ± 6.5	—	—	14.2	17.7	-6.3
	robust	6.5 ± 3.7	—	—			-7.7
SIO1	least squares	-1.2 ± 3.1	10.3 ± 8.2	—	5.2	5.5	-6.4
	robust	0.0 ± 2.8	—	—			-5.2
VNDP	least squares	-13.0 ± 6.3	3.9 ± 5.4	—	-1.1	-1.1	-11.9
	robust	-6.3 ± 4.4	—	—			-5.2

The geodetic model is based on near-field campaign GPS measurements [*Hudnut et al.* 1994]. The seismic/geologic ("S/G") model is based on surface faulting and seismic fault plane solutions [*Bock et al.*, 1993]. Uncertainties are 1σ values.
*Bock et al. [1993] computed vertical displacements relative to JPLM.

and the anomalous vertical displacement at VNDP is less significant. However, the residual vertical motion between the observed vertical displacements and the corresponding model displacements persists.

Preseismic and Postseismic Displacements

The time series of filtered positions prior to the earthquake show no significant short-term preseismic displacements at any of the PGGA sites.

On the basis of high postearthquake displacements in the north component of the baseline GOLD-PIN1 (Figure 4), *Shen et al.* [1992], *Wdowinski et al.* [1992], *Bock et al.* [1993], and *Shen et al.* [1994] postulated postseismic displacements at both sites. The cleaned (unfiltered) time series, which are characterized by a noise level similar to the magnitude of postseismic deformation, do not provide additional information about the individual postseismic displacements of GOLD and PIN1 (Figure 4). Actually, the cleaned series of GOLD shows a very diffuse coseismic and/or postseismic signal. Filtering, however, shows a very pronounced coseismic signal but no postseismic signal. The filtered series of PIN1 shows a postseismic displacement of 6±2 mm (Figures 4 and 6); a similar postseismic displacement is also detected in the north component of the PIN2 and ROCH time series.

We obtain a quantitative characterization of the postseismic deformation by modeling it as a short term exponential relaxation superimposed on a long-term linear interseismic trend. The mathematical description of the model is

$$y(t) = a + b (t - 180) + c \exp [-(t - 180)/\tau] \qquad (10)$$

where y is the relative displacement, t is the time in days since January 1, 1992, a is the intercept, b is the long-term linear trend taken from *Zhang et al.* [1997], c is the magnitude of the postseismic displacement, and τ is the decay time. We use a two-step least squares analysis to evaluate a, c, and τ for each of the three time series (north components of PIN1, PIN2, and ROCH). First, we use the long-term displacement rate from *Zhang et al.* [this issue] to evaluate the intercept a of the three series, excluding the first 10–25 data points suspected of

postseismic displacement. Then we use a least squares fit of the detrended series to evaluate the magnitude c and the decay time τ. Our analysis reveals at all three sites a postseismic displacement of 6±2 mm with decay times of 25±8, 19±8, and 20±10 days at PIN1 (Figure 6b), PIN2, and ROCH, respectively. In order to check our method, we conducted the same procedure on all the other time series and found no significant postseismic displacement in any of them.

Discussion

Improved GPS Data Analysis

Bock et al. [1993] presented seismically induced total far-field displacements for five PGGA sites (GOLD, JPLM, PIN1, SIO1, and VNDP) by averaging 5 weeks of daily site positions before and after the Landers earthquake. Displacements presented by *Blewitt et al.* [1993] at three of the sites agreed with these estimates. Neither study applied, however, integer-cycle phase ambiguity resolution in the GPS data analysis. Therefore their scatter in the east component is more than twice as high as the scatter in the north component. *Wdowinski et al.* [1992] and *Bock et al.* [1993] reported apparent postseismic displacements derived from the baseline time series between the two PGGA sites (GOLD and PIN1) closest to the earthquake's epicenter. They noted for the postearthquake time series an increase in data scatter which they attributed to a possible meteorological effect.

In this study, continuous data from seven PGGA sites are processed by an improved procedure that includes (1) a distributed analysis of global and regional GPS data [*Zhang*, 1996]; (2) an improved mathematical model [*King and Bock*, 1995]; (3) an updated terrestrial reference frame, ITRF93 [*Boucher et al.*, 1994]; (4) integer-cycle phase ambiguity resolution [*Dong and Bock*, 1989; *Feigl et al.*, 1993], and (5) a new spatial filtering technique. Ambiguity resolution results in a much reduced scatter in the east component. The spatial filtering technique increases significantly the signal-to-noise ratio of estimated daily site positions, in particular in the vertical and east components. These five improvements reduced significantly the daily scatter observed after the earthquakes by *Bock et al.* [1993].

(a) PFO Laser Strain Meter

(b) PIN1 Continuous GPS (PFO)
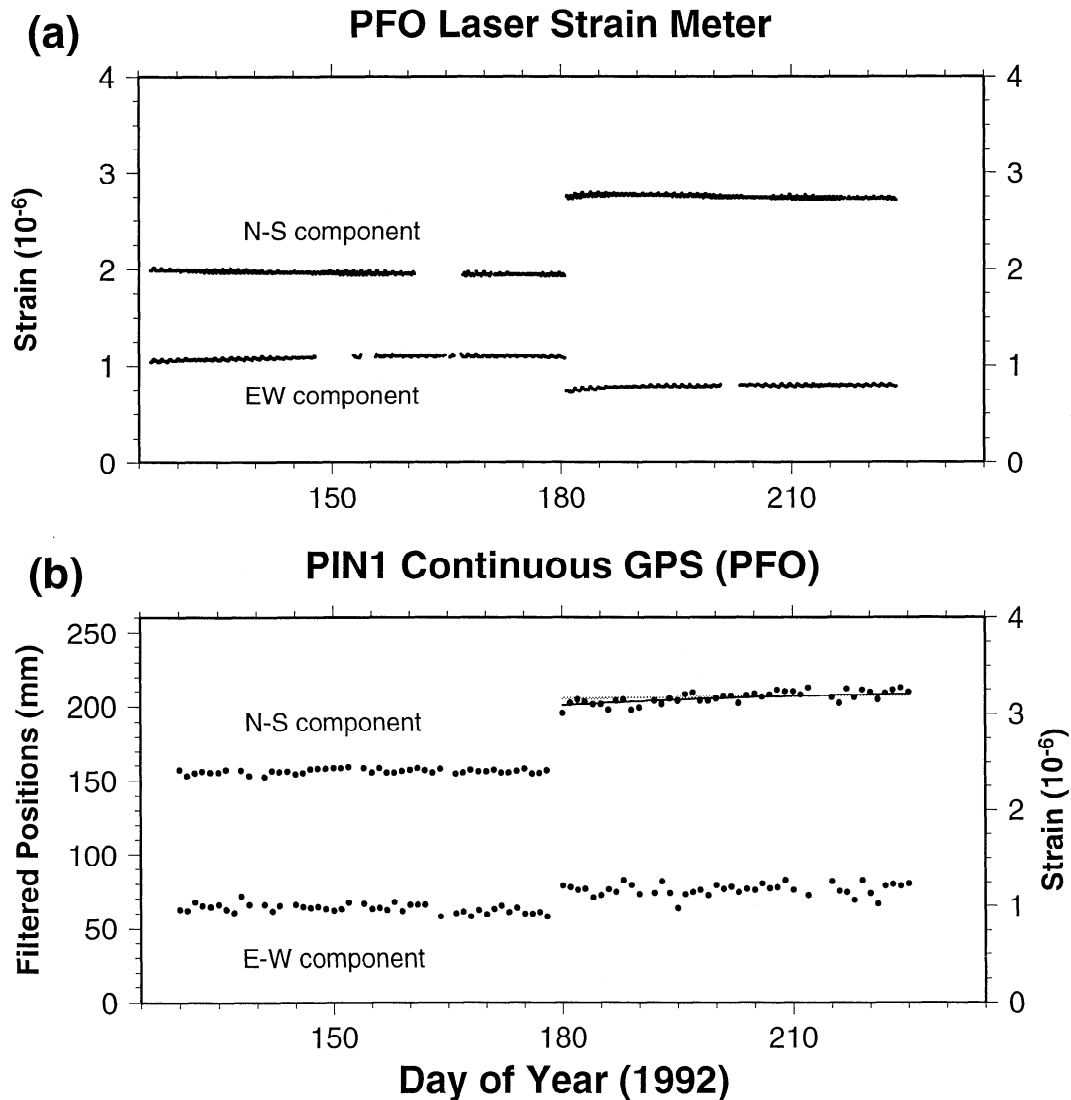
Figure 6. (a) Coseismic and postseismic strain and displacement as observed at Piñon Flat Observatory. The strain scale on the right-hand side of the displacement plot is obtained by scaling the GPS observations with the distance of the station (PIN1) to the Landers earthquake epicenter (~65 km). (b) Solid black line through the postearthquake data represents the best fitting postseismic relaxation model (22 days decay time), and the gray line represents the linear fit of the data using the long-term slope computed by *Zhang et al.* [this issue].

Spatial Filtering

The common-mode signature seen in all the PGGA time series results from global geodetic errors that affect each site within a region in a similar manner, in particular orbital and reference frame errors. Since it is unlikely to be of local tectonic origin, this bias can be removed from each time series resulting in lower RMS scatter in the filtered time series (Figure 3b) compared to the cleaned series (Figure 3a). This method enables detection of transient tectonic signals at individual sites at a level of 2–3 mm, sufficient to distinguish between coseismic and postseismic displacements for the Landers earthquake. However, the method should be used with caution because it neglects any tectonic origin of the common-mode bias. Therefore, in case of coseismic displacement the method should be applied separately to the time series segments before and after the day of the earthquake. Detecting a postseismic signal requires an extra careful usage of the method in order not to smear the signal.

The filtered time series are offset daily in absolute position with respect to the terrestrial reference frame (ITRF93) by the daily common bias removed from all series, which may differ from day to day. Strictly speaking, on any given day the position of each site is expressed with respect to a regional reference frame, rather than with respect to an individual site in traditional relative (baseline) positioning. Nevertheless, on average, the filtered time series still represent "absolute" positions with respect to the terrestrial reference frame. The two major advantages of the filtered series with respect to baseline time series are (1) the filtered series are characterized by a lower RMS scatter than baseline time series (e.g., Figure 4), because the noise level of the latter reflects the residual noise of two sites only, and (2) the filtered series allow the detection of transient signals at a site with respect to the entire region. Detection of individual site displacement is critical for the tectonic implications of the observations, which are used to constrain theoretical calculations (e.g., forward elastic dislocation models) of site displacement.

Coseismic Deformation

Tables 1 and 2 show a comparison between the coseismic movements detected by this study, *Blewitt et al.* [1993], *Bock et al.* [1993], *Freymueller et al.* [1994], and two elastic dislocation models. The "geodetic" model [*Hudnut et al.*, 1994] is based on repeated GPS measurements, before and after the earthquake at 92 stations of which many are located close to the fault trace. Because these measurements detected the total seismically induced displacements, the geodetic model represents the total displacement induced by the earthquakes. The "seismic/geologic" model [*Bock et al.*, 1993] is based primarily on seismic observations and therefore represents only the coseismic displacements. Our results are characterized by significantly lower uncertainties in the east (1–2 mm) and vertical (2–4 mm) components, reflecting improved processing of the data. Owing to our ability to detect a site-specific postseismic signal, we are able to separate total displacement into its coseismic and postseismic components.

Figure 5 shows a comparison between our estimated coseismic displacements and the predicted displacements by the seismic/geologic model. The comparison shows good agreement between the predicted and observed displacements at PIN1, PIN2, and ROCH. The observed displacement at GOLD agrees closely in direction with its predicted value. The magnitude, however, is less than predicted, which supports the conclusion of *Blewitt et al.* [1993] that most of the displacement occurred in the southern section of the fault, while limited displacement occurred in the northern segments. The largest discrepancies are northwest to southwest of the rupture zone at the far-field sites SIO1 and JPLM between the 10–20 mm predicted contour lines and at VNDP well beyond the 10 mm contour. These discrepancies are characterized by a large E-W difference between the observed and predicted values. The poor fit at these sites may reflect the limitations of the dislocation model that assumes a homogeneous elastic half-space. This assumption appears valid for the intermediate epicentral distance but appears to be less accurate in the far field.

All of these studies show similar horizontal displacements indicating that even for a short series (70 days in the two previous studies) these displacements can be determined with an uncertainty of 2–5 mm, without considering interseismic displacements rate. A more precise detection of the coseismic and postseismic displacements as determined here requires consideration of the longer-term interseismic displacement rates.

The vertical displacements are computed by robust estimation with an uncertainty of approximately 2–4 mm. The observed motions are in all cases 5–10 mm more negative than expected by either model. Furthermore, they are not significantly different than those reported by *Blewitt et al.* [1993] and *Freymueller et al.* [1994]. These results suggest that (1) the homogeneous half-space dislocation models are inadequate to model the vertical displacements or (2) the observed vertical displacements may indicate an additional physical process of regional subsidence. Distinguishing between these and other possible explanations is beyond the scope of this paper.

Postseismic Deformation

Significant horizontal postseismic displacements are detected at PIN1, PIN2, and ROCH. They agree with postseismic motion inferred from data collected by the nearby N-S and E-W laser strain meters (Figure 6) [*Wyatt et al.*, 1994]. The postseismic displacements detected at two of the PGGA sites provide, for the first time, a temporally detailed observation of this phenomena with GPS. The 6±2 mm of postseismic motion represents 10–20% of the coseismic displacement. The postseismic signal is modeled as short-term postseismic exponential relaxation with a decay time of 22±10 days superimposed upon a long-term linear rate of displacement. *Wyatt et al.* [1994] observed postseismic strain at PIN1 by laser strain meters (Figure 6a). Their analysis indicates that the postseismic strain lasted 5–6 days following the Landers earthquake and its magnitude was 8% of the coseismic slip. By scaling the geodetically detected coseismic and postseismic displacements with the distance to the epicenter we obtain an independent measure of strain which agrees well with the direction and magnitude of the more precise laser strain meter data (Figure 6).

Shen et al. [1994] used field GPS measurements to observe the postseismic displacement at various sites near the epicenter. They observed postseismic displacements up to 56 mm near the epicenter, and a few mm far from the fault rupture zone. They estimated the postseismic moment release as 15% of the coseismic moment release and a relaxation constant for an exponential decay model of 34 days. Their observations provide a better spatial distribution of postseismic deformation by observing at more sites, and at sites closer to the epicentral region. Because their analysis is based on relative positions, they evaluated the individual site displacement with respect to PIN1, which biased their results by 6±2 mm. *Savage and Svarc* [1997] observed postseismic deformation across the Emerson fault, which ruptured during the Landers earthquake. They detected a short term postseismic exponential relaxation (decay time 84±23 days) superimposed upon a long-term linear trend. Differences in the decay time represent a different crustal response to the earthquake at various locations; however, it may also reflect estimation errors arising from the sparse temporal resolution of their field measurements.

Wyatt et al. [1994] proposed various mechanisms to explain the observed postseismic displacements: hydraulic fracture opening, poroelastic effects, hydrothermal effects, crustal anelasticity, and aseismic fault slip. Supported by earlier results, they ruled out all but the last two of those mechanisms. Our current results, which also show measurable small postseismic displacement at the Piñon Flat Observatory stations, support their conclusion that aseismic after-slip has been distributed differently than the coseismic slip. Our results are also consistent with the interpretation by *Shen et al.* [1994], who suggest that significant afterslip or viscous relaxation occurred below 10 km depth as the rupture zone extended itself into unbroken rock below and along the initial rupture zone.

The detectability of other transient events such as creep events, strain variations, and preseismic deformation by continuous GPS will depend on the magnitude and wavelength of such signals [e.g., *Agnew*, 1992]. Preseismic deformation is elusive, and its existence is only suggested by fragmentary observations of anomalous crustal deformation prior to large earthquakes [*Scholz*, 1990]. Whether other phenomena exist within the earthquake cycle is still a matter of speculation. They will be more difficult to detect since their time of occurrence within the earthquake cycle is unknown.

Conclusions

A new spatial filtering method was developed to detect surface displacements induced by the June 28, 1992 Landers earthquake. This new method enables us to partition total surface displacement into its coseismic and postseismic components. We detect significant coseismic displacements at all 7 PGGA sites that operated continuously in southern California during the 100-day period centered on the earthquake. Postseismic displacements are detected only at the three sites closest to the epicenter. The coseismic horizontal displacements lie in the range of 5–65 mm, with uncertainties of 1–2 mm, and are in general agreement with elastic dislocation models. The vertical displacements lie in the range from -13 to +7 mm, with uncertainties of 2–4 mm. However, these displacements are systematically 5–10 mm more negative than expected from elastic dislocation models. The postseismic horizontal displacements are of magnitude 6 ± 2 mm, which represents 15% of the coseismic displacement. The postseismic signal is modeled as short-term post-seismic exponential relaxation with a decay time of 22 ± 10 days superimposed upon a long-term linear rate of displacement. Scaling the coseismic and postseismic displacements at Piñon Flat Observatory with the distance to the epicenter provides an independent measure of site strain, which agrees well with strain meter data. Thus, we see that continuous GPS measurements are well suited for accurately detecting coseismic and postseismic deformation.

References

Agnew, D. C., The time domain behavior of power-law noises, *Geophys. Res. Lett., 19,* 333-336, 1992.

Blewitt, G., M. B. Heflin, K. J. Hurst, D. C. Jefferson, F. H. Webb, and J. F. Zumberge, Absolute far-field displacements from the June 28, 1992, Landers earthquake sequence, *Nature, 361,* 340-342, 1993.

Bock, Y., Continuous monitoring of crustal deformation, *GPS World, 2 (6),* 40-47, 1991.

Bock, Y., et al., Detection of crustal deformation from the Landers earthquake sequence using continuous geodetic measurements, *Nature, 361,* 337-340, 1993.

Bock, Y., et al., Southern California Permanent GPS Geodetic Array: Continuous measurements of crustal deformation between the 1992 Landers and 1994 Northridge earthquakes, *J. Geophys. Res.,* this issue.

Boucher, C., Z. Altamimi, and L. Duhem, Results and analysis of the ITRF93, *IERS Tech. Note 18,* Int. Earth Rotation Serv., Obs. de Paris, 1994.

Dong, D., and Y. Bock, Global Positioning System network analysis with phase ambiguity resolution applied to crustal deformation studies in California, *J. Geophys. Res., 94,* 3949-3966, 1989.

Feigl, K. L., et al., Space geodetic measurement of crustal deformation in central and southern California, 1984-1992, *J. Geophys. Res., 98,* 21,677-21,712, 1993.

Freymueller, J., N. E. King, and P. Segall, The co-seismic slip distribution of the Landers earthquake, *Bull. Seismol. Soc. Am., 84,* 646-659, 1994.

Happer, J., D. Agnew, Y. Bock, H. Johnson, K. Stark, F. Wyatt and D. Jackson, Results from continuous GPS measurements over a 14-km line, *Eos Trans. AGU, 72 (17),* Spring Meet. Suppl., 118, 1991.

Hauksson, E., et al., Overview of the 1992 ($M6.1,7.5,6.6$) Landers earthquake sequence in San Bernadino County, California, *Eos Trans. AGU, 73,* 357, 1992.

Herring, T. A., Documentation of the GLOBK Software version 3.3, Mass. Inst. of Technol., Cambridge, 1995.

Hudnut, K. W., et al., Coseismic displacements of the 1992 Landers earthquake sequence, *Bull. Seismol. Soc. Am., 84,* 625-645, 1994.

Johnston, M. J. S., A. T. Linde, and D. C. Agnew, Continuous borehole strain in the San Andreas fault zone before, during, and after the 28 June 1992, M_W 7.3 Landers, California, earthquake, *Bull. Seismol. Soc. Am., 84,* 799-805, 1994.

Kanamori, H., H-K. Thio, D. Dreger, and E. Hauksson, Initial investigation of the Landers, California, earthquake of 28 June 1992 using TERRAscope, *Geophys. Res. Lett., 19,* 2267-2270, 1992.

King, R. W., and Y. Bock, Documentation of the GAMIT GPS Analysis Software version 9.3, Mass. Inst. of Technol., Cambridge, 1995.

Landers Earthquake Response Team, Near-field investigations of the Landers earthquake sequence, April to July, 1992, *Science, 260,* 171-176, 1993.

Massonnet, D., M. Rossi, C. Carmona, F. Adragna, G. Peltzer, K. Feigl, and T. Rabaute, The displacement field of the Landers earthquake mapped by radar interferometry, *Nature, 364,* 138-142, 1993.

Massonnet, D., K. Feigl, M. Rossi, and F. Adragna, Radar interferometric mapping of deformation in the year after the Landers earthquake, *Nature, 369,* 227-230, 1994.

Press, W. H., B. P. Flannery, S. A. Teukolsky, and W. T. Vetterning, *Numerical Recipes in C, The Art of Scientific Computing,* Cambridge Univ. Press, New York, 1988.

Savage, J. C., and J. L. Svarc, Postseismic deformation associated with the 1992 M_W=7.3 Landers earthquake, southern California, *J. Geophys. Res., 102,* 7565-7577, 1997.

Scholz, C. H., *The Mechanics of Earthquakes and Faulting,* Cambridge Univ. Press, New York, 1990.

Shen, Z.-K., Y. Feng, M. Cline, and D. D. Jackson, Post-seismic deformation following Landers and Big Bear earthquakes, California, June 28, 1992, *Eos Trans. AGU, 73 (43),* Fall Meet. Suppl., 365, 1992.

Shen, Z.-K., D. D. Jackson, Y. Feng, M. Cline, M. Kim, P. Fang and Y. Bock, Postseismic deformation following the Landers earthquake, California, June 28, 1992, *Bull. Seismol. Soc. Am., 84,* 780-791, 1994.

Wdowinski, S., Y. Bock, P. Fang, J. F. Genrich, D. C. Agnew and F. K. Wyatt, The 1992 Landers earthquake sequence: Detection of coseismic and postseismic surface displacement, *Eos Trans. AGU, 73 (43),* Fall. Meet. Suppl., 364, 1992.

Wessel, P., and W. H. F. Smith, Free software helps map and display data, *Eos Trans. AGU, 72,* 445-446, 1991.

Wyatt, F. K., H. Bolton, S. Bralla, and D. C. Agnew, New designs of geodetic monuments for use with GPS, *Eos Trans. AGU, 70,* 1054-1055, 1989.

Wyatt, F. K., D. C. Agnew, and M. Gladwin, Continuous measurements of crustal deformation for the 1992 Landers earthquake sequence, *Bull. Seismol. Soc. Am., 84,* 768-779, 1994.

Zebker, H. A., P. A. Rosen, and R. M. Goldstein, On the derivation of coseismic displacement fields using differential radar interferometry: The Landers earthquake, *J. Geophys. Res., 99,* 19,617-19,634, 1994.

Zhang, J., Continuous GPS measurements of crustal deformation in southern California, Ph.D. dissertation, Univ. of Calif., San Diego, 1996.

Zhang, J., Y. Bock, H. Johnson, P. Fang, J. Genrich, S. Williams, S. Wdowinski, and J. Behr, Southern California Permanent GPS Geodetic Array: Error analysis of daily position estimates and site velocities, *J. Geophys. Res.*, this issue.

Y. Bock, P. Fang, J. Genrich, and J. Zhang, Cecil H. and Ida M. Green Institute of Geophysics and Planetary Physics, Scripps Institution of Oceanography, 9500 Gilman Drive, La Jolla, CA 92093. (email: ybock@ucsd.edu; pfang@pgga.ucsd.edu; jeff@pgga.ucsd.edu; jie@illustra.com)

S. Wdowinski, Department of Geophysics and Planetary Physics, Tel Aviv University, Ramat Aviv, 69978, Israel. (shimon@geo1.tau.ac.il)